Langmuir
Article
pubs.acs.org/Langmuir
© 2010 American Chemical Society

Lyotropic Liquid Crystalline Self-Assembly in Dispersions of Silver Nanowires and Nanoparticles

Shanthi Murali, Teng Xu, Bennett D. Marshall, Matthew J. Kayatin, Khristine Pizarro, Vinod K. Radhakrishnan, Dhriti Nepal, and Virginia A. Davis*

Department of Chemical Engineering, Auburn University, Auburn, Alabama 36849

Received September 5, 2009. Revised Manuscript Received May 13, 2010

We report demixed nematic lyotropic liquid crystalline phase formation in dispersions of silver nanowires and spherical nanoparticle aggregates in ethylene glycol and water. This phase is observed in samples in spite of the high density, large aspect ratio, and long relaxation times of the nanowires which have an average length of 6.8 μm. Remarkably, in the biphasic region, the nanowire-rich liquid crystalline phase exhibits a strandlike morphology which has only previously been reported for single-walled carbon nanotube liquid crystals. Shearing predominantly liquid crystalline dispersions results in both significant nanowire alignment and nanowire−aggregate demixing. The results of this research suggest that the nanoparticle contaminants common to many synthesis schemes facilitate liquid crystalline phase formation and that these dispersions can be processed into aligned coatings.

Introduction

Throughout the greater than 130 year history of liquid crystalline science, the discovery of new materials has repeatedly led to both enhanced scientific understanding and breakthrough applications. The discovery of small organic molecule thermotropic liquid crystals continues to enable increasingly sophisticated liquid crystalline displays. Similarly, the discovery of rodlike macromolecules led to the discovery of their lyotropic liquid crystalline phases and the development of processing routes to produce high-strength polymer fibers from their lyotropic liquid crystalline dispersions.[1] More recently, the discovery of scalable synthesis routes for 1-dimensional nanocylinders such as carbon nanotubes and inorganic nanorods, nanotubes, and nanowires have sparked new opportunities to both increase fundamental understanding of liquid crystalline assembly and develop processing routes for producing highly aligned materials from liquid crystalline dispersions. Based on theories for fluid dispersed rods, at low volume fractions rods exist in a dilute regime where they can rotate and translate freely due to Brownian motion without interference from another rod. While one normally considers Brownian particles as small, low aspect ratio entities, it has recently been shown that even 20 nm diameter germanium nanowires with lengths up to 10 μm undergo Brownian motion in low-viscosity fluids.[2] As concentration is increased, the system transitions to a semidilute regime where translation is inhibited to an isotropic concentrated regime where both rotation and translation are inhibited.[3] At a critical concentration ϕ_I, the system becomes biphasic; a portion of the rods remain in an isotropic phase, and a portion form liquid crystalline domains. The liquid crystalline phase formation is the result of the loss in orientational entropy being compensated by the gain in translational entropy.[4] With further increases in concentration, the liquid crystalline phase will become increasingly dominant until the system becomes fully liquid crystalline at a second critical concentration ϕ_N. According to Onsager theory[4] for monodisperse spherocylinders with only hard-rod interactions, $\phi_I = 3.34/(L/D)$ and $\phi_N = 4.49/(L/D)$, where L is the rod length and D is the diameter.

In contrast to polymeric,[1] and even carbon nanotube,[5] lyotropic liquid crystals, relatively little is known about the phase behavior and shear response of lyotropic liquid crystals composed of inorganic cylinders. Lyotropic liquid crystalline phase formation was reported for vanadium pentoxide sols as early as 1915,[6] but as of the late 1990s only about a dozen completely inorganic, or mineral liquid crystalline, phases had been discovered.[7] The historically limited interest in inorganic liquid crystals has been attributed to several factors including the size polydispersity of inorganic rodlike materials and a perceived lack of interesting applications compared to their organic cousins.[8] However, inorganic nanocylinders' (e.g., nanowires', nanorods', nanotubes') exciting properties have created new interest in their liquid crystalline self-assembly; lyotropic liquid crystalline phases have recently been reported in dispersions of boehmite,[9] goethite,[10] rutile,[11] CdSe,[12] gold,[13−15] and polymer-functionalized TiO_2[16] nanocylinders. These systems demonstrate that it is possible to

*Corresponding author. E-mail: davisva@auburn.edu.

(1) Donald, A. M.; Windle, A. H. *Liquid Crystalline Polymers*; Cambridge University Press: Cambridge, 1992.
(2) Marshall, B. D.; Davis, V. A.; Lee, D. C.; Korgel, B. A. *Rheol. Acta* **2009**, *48* (5), 589–596.
(3) Doi, M.; Edwards, S. F. *The Theory of Polymer Dynamics*; Oxford University Press: Oxford, 1986.
(4) Onsager, L. *Ann. N.Y. Acad. Sci.* **1949**, *51*, 627–659.
(5) Zakri, C.; Poulin, P. *J. Mater. Chem.* **2006**, *16*(42), 4095–4098.
(6) Diesselhorst, H.; Freundlich, H.; Leonard, B. *Elster-Geitel-Fortschrift* **1915**, *180*, 453.
(7) Gabriel, J. C. P.; Davidson, P. *Adv. Mater.* **2000**, *12*(1), 9–20.
(8) Davidson, P.; Batail, P.; Gabriel, J. C. P.; Livage, J.; Sanchez, C.; Bourgaux, C. *Prog. Polym. Sci.* **1997**, *22*(5), 913–936.
(9) Bruggen, M. P. B. v.; Kooij, F. M. v. d.; Lekkerkerker, H. N. W. *J. Phys.: Condens. Matter* **1996**, *8*(47), 9451–9456.
(10) Vroege, G. J.; Thies-Weesie, D. M. E.; Petukhov, A. V.; Lemaire, B. J.; Davidson, P. *Adv. Mater.* **2006**, *18*(19), 2565–2568.
(11) Dessombz, A.; Chiche, D.; Davidson, P.; Panine, P.; Chaneac, C.; Jolivet, J. P. *J. Am. Chem. Soc.* **2007**, *129*(18), 5904–5909.
(12) Li, L. S.; Walda, J.; Manna, L.; Alivisatos, A. P. *Nano Lett.* **2002**, *2*(6), 557–560.
(13) Murphy, C. J.; San, T. K.; Gole, A. M.; Orendorff, C. J.; Gao, J. X.; Gou, L.; Hunyadi, S. E.; Li, T. *J. Phys. Chem. B* **2005**, *109*(29), 13857–13870.
(14) Jana, N. R.; Gearheart, L. A.; Obare, S. O.; Johnson, C. J.; Edler, K. J.; Mann, S.; Murphy, C. J. *J. Mater. Chem.* **2002**, *12*(10), 2909–2912.
(15) Sharma, V.; Park, K.; Srinivasarao, M. *Mater. Sci. Eng., R* **2009**, *65*(1−3), 1–38.
(16) Meuer, S.; Oberle, P.; Theato, P.; Tremel, W.; Zentel, R. *Adv. Mater.* **2007**, *19*(16), 2073–2078.

overcome the challenges of achieving inorganic nanocylinder liquid crystalline phases and provide a foundation for ongoing research. As with many nanoscale systems, one of the most significant challenges is dispersion. Inorganic nanocylinders can be difficult to disperse in solvents at a sufficient volume fraction for liquid crystalline phase formation. One issue is that the high density of the nanocylinders results in the need for very high mass fractions in order to achieve the required volume fraction for liquid crystalline phase formation. The volume fraction ϕ is defined as

$$\phi = \frac{\rho_{rel} w}{1 + (\rho_{rel} - 1) w}$$
$$\rho_{rel} = \rho_{solvent} / \rho_{rod} \quad (1)$$

where w is the weight fraction of the rod.

Inorganic nanocylinder dispersions' kinetic stability is affected by several factors including sedimentation, long-range attractive interactions,[17,18] and rod polarizability.[19] In the 60 years since Onsager's seminal work,[4] numerous theories have been developed to account for rod−rod and rod−solvent interactions[1,20,21] as well as rod length polydispersity.[1,22−25] However, even for relatively simple systems, challenges remain in predicting the experimental phase behavior of polydisperse rods with complex interactions.[26] Furthermore, while inorganic nanocylinders can be produced with very controlled aspect ratios, many of the more scalable nanocylinder synthesis schemes for high aspect ratio nanocylinders result in length polydispersity and a high number fraction of spherical and even cubic nanoparticles.[27−30] Both size and shape polydispersity significantly increase the phase behavior complexity, and while there have been many theoretical studies of liquid crystal phase formation in the presence of rods and spheres, there have been few experimental studies. Notable exceptions include ten Brinke et al.'s recent investigations of the effects of the presence of different shapes on the rheological properties of colloidal clay particles[31,32] and Dogic and Fraden's investigations of mixtures of spheres and *fd* virus.[33] Even the liquid crystalline phases that have been achieved are comprised of a polydomain structure where each domain is oriented along a different director. This is similar to other macromolecular liquid crystals such as rodlike polymers and SWNTs, but in contrast to small molecule thermotropic liquid crystals where a monodomain structure can be achieved on short time scales. While thermodynamics drives macromolecular liquid crystal's polydomain structure toward a uniformly monodomain structure, the long relaxation times and high viscosities resulting from the large aspect ratio mean that this process can take months or years to complete.[34] For this reason, external shear or magnetic or electrical fields must be used to achieve uniform orientation.[1] Among these, shear is particularly attractive because it is inherent in most liquid phase processing techniques. A notable example of the use of shear to improve alignment in solid materials produced from liquid crystalline dispersions is DuPont Kevlar. This high-strength fiber is produced by solution spinning a liquid crystalline dispersion of polyphenylene terephthalamide (PPTA) in H_2SO_4; the shear in the spinneret as well as drawing enhances the alignment. More recently, Davis et al. and Ericson et al. demonstrated the liquid crystalline phase behavior of single-walled carbon nanotubes (SWNTs) in superacids and the processing of these phases into highly aligned fibers; the final degree of alignment was found to be shear dependent.[17,35−37] Similarly, Song and Windle demonstrated liquid crystalline processing of carboxylated multiwalled carbon nanotubes (MWNTs) in water.[38]

We report the liquid crystalline phase behavior of a mixture of polyvinylpyrrolidone (PVP)-coated silver nanowires and nanoparticles dispersed in ethylene glycol (Ag−EG) and water (Ag−H_2O). To the authors' knowledge, this is the first experimental observation of liquid crystalline phase formation in a dispersion comprised of both high aspect ratio inorganic nanocylinders and nanoparticles; the nanoparticles partition to a separate phase and enable nanocylinder liquid crystal phase formation at lower than expected concentrations. We further show how the presence of aligned domains in the dispersion facilitates alignment in silver coatings. Because of silver's excellent electrical, optical, thermal, and antimicrobial properties, such coatings are promising materials for a range of applications including surface-enhanced Raman scattering (SERs) substrates, optoelectronic devices, antimicrobial surfaces, and biomedical devices.[39−43]

Experimental Section

Synthesis. Silver nanowires were synthesized using the microwave-assisted polyol method described by Gou et al.[27] Although this method quickly produces a large quantity of nanowires, it produces a large number of polyvinylpyrrolidone (PVP)-coated nanoparticle aggregates which are roughly spherical in shape and difficult to separate from the nanowires. In a typical experiment, 110 mg of PVP (MW 58 000), 90 mg of silver nitrate ($AgNO_3$), and 5 mg of sodium chloride (NaCl) were added to 20 mL of ethylene

(17) Davis, V. A.; Ericson, L. M.; Parra-Vasquez, A. N.; Fan, H.; Wang, Y.; Prieto, V.; Longoria, J. A.; Ramesh, S.; Saini, R.; Kittrell, C.; Billups, W. E.; Adams, W. W.; Hauge, R. H.; Smalley, R. E.; Pasquali, M. *Macromolecules* **2004**, *37*(1), 154–160.
(18) Israelachvili, J. N. *Intermolecular and Surface Forces*, 2nd ed.; Academic Press: London, 1992.
(19) Ghezelbash, A.; Koo, B.; Korgel, B. A. *Nano Lett*. **2006**, *6*(8), 1832–1836.
(20) Flory, P. J. *Proc. R. Soc. London, Ser. A* **1956**, *234*, 73–89.
(21) Khokhlov, A. R. Theories Based on the Onsager Approach. In *Liquid Crystallinity in Polymers*; Ciferri, A., Ed.; VCH Publishers: New York, 1991; pp 97−129.
(22) Speranza, A.; Sollich, P. *J. Chem. Phys*. **2002**, *117*(11), 5421–5436.
(23) Speranza, A.; Sollich, P. *Phys. Rev. E* **2003**, *67*(6), 061702/1–061702/19.
(24) Speranza, A.; Sollich, P. *J. Chem. Phys*. **2003**, *118*(11), 5213–5223.
(25) Wensink, H. H.; Vroege, G. J. *J. Chem. Phys*. **2003**, *119*(13), 6868–6882.
(26) Dogic, Z.; Purdy, K. R.; Grelet, E.; Adams, M.; Fraden, S. *Phys. Rev. E* **2004**, *69* (5).
(27) Gou, L. F.; Chipara, M.; Zaleski, J. M. *Chem. Mater*. **2007**, *19*(7), 1755–1760.
(28) Sun, Y. G.; Yin, Y. D.; Mayers, B. T.; Herricks, T.; Xia, Y. N. *Chem. Mater*. **2002**, *14*(11), 4736–4745.
(29) Sun, Y. G.; Xia, Y. N. *Adv. Mater*. **2002**, *14*(11), 833–837.
(30) Sharma, V.; Park, K.; Srinivasarao, M. *Proc. Natl. Acad. Sci. U.S.A*. **2009**, *106*(13), 4981–4985.
(31) ten Brinke, A. J. W.; Bailey, L.; Lekkerkerker, H. N. W.; Maitland, G. C. *Soft Matter* **2008**, *4*(2), 337–348.
(32) ten Brinke, A. J. W.; Bailey, L.; Lekkerkerker, H. N. W.; Maitland, G. C. *Soft Matter* **2007**, *3*(9), 1145–1162.
(33) Dogic, Z.; Fraden, S. *Soft Matter* **2006**, *2*, 1–86.
(34) Larson, R. G. *The Structure and Rheology of Complex Fluids*; Oxford University Press: New York, 1999.
(35) Ericson, L. M. Macroscopic Neat Single-Wall Carbon Nanotube Fibers. PhD Dissertation, Rice University, Houston, 2003.
(36) Ericson, L.; Fan, H.; Peng, H.; Davis, V.; Zhou, W.; Sulpizio, J.; Wang, Y.; Booker, R.; Vavro, J.; Guthy, C.; Parra-Vasquez, A.; Kim, M.; Ramesh, S.; Saini, R.; Kittrell, C.; Lavin, G.; Schmidt, H.; Adams, W.; Billups, W.; Pasquali, M.; Hwang, W.; Hauge, R.; Fischer, J.; Smalley, R. *Science* **2004**, *305*(5689), 1447–1450.
(37) Davis, V. A.; Parra-Vasquez, A. N. G.; Green, M. J.; Rai, P. K.; Behabtu, N.; Prieto, V.; Booker, R. D.; Schmidt, J.; Kesselman, E.; Zhou, W.; Fan, H.; Adams, W. W.; Hauge, R. H.; Fischer, J. E.; Cohen, Y.; Talmon, Y.; Smalley, R. E.; Pasquali, M. *Nat. Nanotechnol*. **2009**, *4*(12), 830–834.
(38) Song, W.; Kinloch, I. A.; Windle, A. H. *Science* **2003**, *302*(5649), 1363.
(39) Pang, Y. T.; Meng, G. W.; Fang, Q.; Zhang, L. D. *Nanotechnology* **2003**, *14* (1), 20–24.
(40) Hu, X. H.; Chan, C. T. *Appl. Phys. Lett*. **2004**, *85*(9), 1520–1522.
(41) Jeong, D. H.; Zhang, Y. X.; Moskovits, M. *J. Phys. Chem. B* **2004**, *108*(34), 12724–12728.
(42) Aslan, K.; Lakowicz, J. R.; Geddes, C. D. *Anal. Bioanal. Chem*. **2005**, *382* (4), 926–933.
(43) De, S.; Higgins, T. M.; Lyons, P. E.; Doherty, E. M.; Nirmalraj, P. N.; Blau, W. J.; Boland, J. J.; Coleman, J. N. *ACS Nano* **2009**.

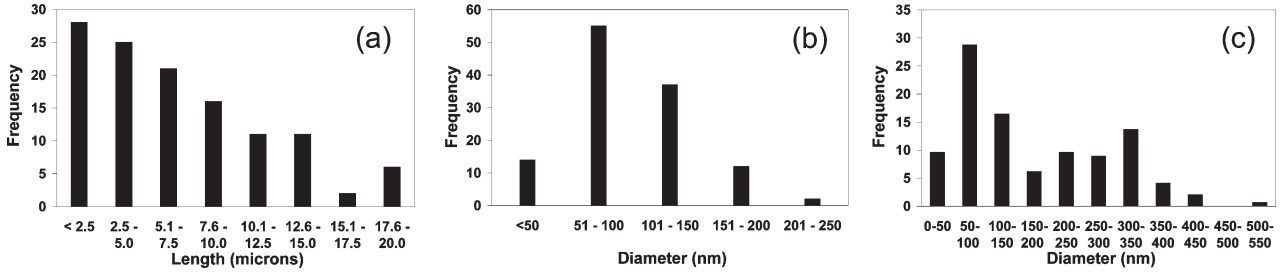

Figure 1. Histogram of (a) lengths and (b) diameters of 120 nanowires prepared at power level 3 for 3.5 min. The average nanowire length is 6.8 μm, and the average diameter is 100 nm. (c) Histogram of nanoparticle aggregate diameters.

glycol (EG); all chemicals were purchased from Sigma-Aldrich (Milwaukee, WI) and used as received. The mixture was bath sonicated for 5 min in a 55 kHz Cole-Parmer bath sonicator in order to accelerate the dispersion process. During sonication the appearance changed from colorless to opalescent as a result of the conversion of silver nitrate to silver chloride. The sonicated mixture was heated in a household General Electric 1.1 ft^3 capacity countertop microwave for 3.5 min at a power level of 3. The conversion of the silver ions to solid nanomaterials, the length of the resulting nanorods, and the fraction of nanocylinders compared to nanoparticles could be tailored by changing the power level (frequency of magnetron oscillating on and off) and the total heating time. Research grade microwaves with constant power input were found to provide little advantage since rapid heating, even at low wattages, resulted in rapid nanoparticle seed formation and breakdown of nanowires back into particulates. It should be noted that caution should be used during and after microwave heating. The dispersions heat rapidly to the ethylene glycol boiling point of 197 °C, and care must be taken to avoid boiling over the solution or creating a significant quantity of potentially ignitable vapor in the microwave. The dispersions should also be allowed to cool before handling to avoid the potential for burns and inhaling EG vapor.

Separation of Nanoparticle Aggregates and Nanowires. Several approaches for increasing the number fraction of nanowires to nanoparticle aggregates were investigated. In the majority of this research, the as-synthesized samples were simply allowed to sediment overnight; this resulted in a top portion consisting primarily of nanoparticle aggregates and sediment portion containing both self-assembled nanowires and nanoparticle aggregates. In a second approach, the entire sample centrifuged in a Cole-Parmer ultracentrifuge at 5000 rpm for 5 min, and a portion or all of the sediment was removed. In some cases, the Ag was transferred to water by first washing with acetone to remove the excess PVP and EG, centrifuging as above, redispersing the residue in water, and repeating the process several times. In another approach, the sample was simply vacuum filtered through a 3 μm polycarbonate filter.

Characterization. To determine the concentration of dilute dispersions, UV−vis spectroscopy was carried out in a Varian 300E spectrophotometer using a 1 cm quartz cuvette. For higher concentration samples, thermogravimetric analysis (TGA) was performed in a TA Instruments Q-500 thermal gravimetric analyzer. The sample was heated in clean platinum pans at 5 °C/min to 500 °C under a constant nitrogen balance protection flow rate of 40 cm^3/min and sample air flow rate of 60 cm^3/min. Differential scanning calorimetry (DSC) was performed on a TA Instruments Q-2000 in hermetically sealed aluminum pans at a scan rate of 5 °C/min over a temperature range of −60 to 20 °C with three thermal cycles of heating, cooling, and reheating. Rheology was performed using an Anton Paar MCR 301 rotational rheometer at 20 °C using 25 mm parallel plates. Morphology was characterized using a Zeiss EM 10 transmission electron microscope to image dried drops on carbon-coated copper grids, and a JEOL 7000F FE-SEM with EDX detector was used to characterize drops dried directly on SEM stubs. Optical imaging was performed in transmission using a Nikon Eclipse 80i optical microscope equipped with cross-polarized differential interference contrast (DIC), a Retiga camera, and digital imaging workstation with Image Pro software. Two optical microscopy sample preparation methods were used. In one method, ~20 μL of sample was placed between a microscope slide and cover glass and then sealed. In another method, the sample was drawn into a Vitrocom capillary tube 0.2 mm height, 2 mm in width, and 5 cm in length, and then the tube ends were sealed. A Renishaw inVia Raman spectrometer was used to verify the presence of PVP on the silver after washing in water and acetone and to characterize the alignment of dry shear-aligned films using a 514 nm laser and 50× objective.

Results and Discussion

Synthesis. The microwave-assisted polyol method has the key advantage of being able to produce a significant number of nanowires in a short amount of time. A setting of power level 3 and 3.5 min of total time was found to produce the highest number fraction of nanowires compared to nanoparticle aggregates, but the number fraction of nanowires was typically less than 0.10. At these conditions, the dispersions could be qualitatively characterized by their light brown color and slightly shiny appearance (image available in the Supporting Information). Consistent with the findings of Gou et al., both higher power levels and longer times resulted in both shorter and a lower percentage of nanowires due to the competition amongst seed formation, nanowire growth, and dissolution reactions.[27] This competition likely also contributes to the nanowire size polydispersity. TEM measurements made on 120 nanowires revealed a broad distribution of both lengths and diameters (Figure 1) with an average length $L = 6.8\ \mu$m and average diameter $D = 100$ nm. This results in an average aspect ratio of $L/D = 68$. TEM and SEM also showed that what appeared to be nanoparticles using optical microscopy were actually large, roughly spherical, aggregates of spherical and cubic nanoparticles overcoated with a layer of PVP. The total diameter of these nanoparticle aggregates varied widely but was typically several times larger than that of the nanowires. A representative histogram is shown in Figure 1, and images are available in the Supporting Information. It should be noted that there was no correlation between the nanowire length and diameter.

The large and polydisperse diameters of the nanoparticle aggregates made separation difficult. Although complete removal of nanoparticles by centrifugation and washing is theoretically possible, the process is tedious and complete separation was never observed even after repeated centrifugation and washing steps. Because of the size and shape of nanoparticle aggregates and nanowires, the relative sedimentation forces result in the nanoparticle aggregates concentrating near the bottom of the centrifuge tube.[30] The nanowires, on the other hand, accumulate on the sidewall, particularly near the tangent line (image available in Supporting Information). Harvesting only this region of the sediment resulted in nanowire number fractions as high as 0.5,

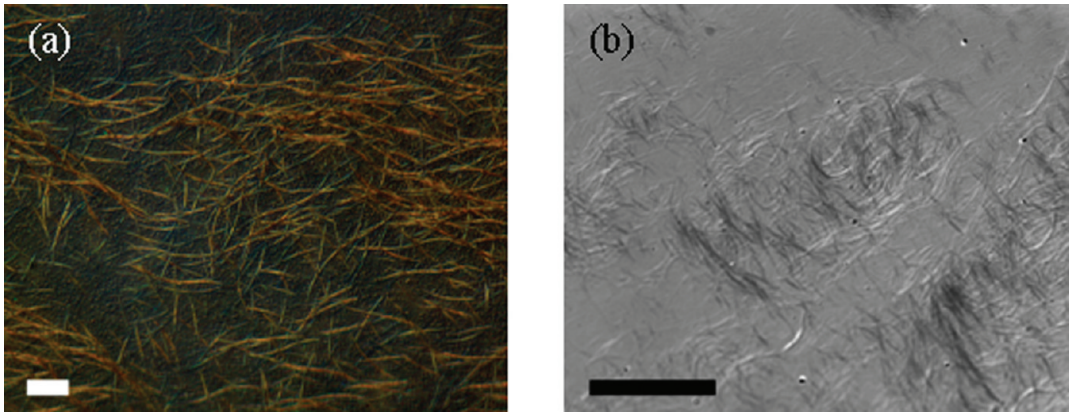

Figure 2. (a) Color transmission microscopy image of birefringent silver nanowires strands observed in a capillary tube under partially cross-polarized light using a 20× DIC 0.45 NA objective and 2× additional magnification in front of the camera. Imaging successive planes shows that the strands are continuous and weave in and out of multiple focal planes while the nanoparticles have segregated to a lower focal plane. (b) Biphasic dispersion of SWNTs in 102% H_2SO_4, called SWNT "spaghetti", under partially crossed polarizers using a 63× DIC 1.4 NA oil immersion objective with 2.5× magnification in front of the camera (modified from ref 17). Scale bars are 20 μm in both images.

but the number fractions varied widely depending on exactly which part of the sediment was removed. This method also yielded very little material. While centrifugation speed and time theoretically improve separation, it should be noted that longer or more rapid centrifugation resulted in the formation of additional aggregates due to nanowire breakage. Filtration and sedimentation are easier, higher yield methods, but the results from filtration were inconsistent possibly due to differences in the structure formed by the accumulation of nanowires on the filter paper and the extent to which that structure prevents the spherical aggregates from passing through. The simplest method, sedimentation, produced the most consistent results with a nanowire to nanoparticle aggregate ratio of 0.2. Additional information on average nanowire and nanoparticle aggregate sizes and number fraction of nanowires after different types of processing is given in the Supporting Information.

Liquid Crystalline Self-Assembly. Cross-polarized microscopy of the Ag−EG sediments formed without any washing or centrifugation showed significant evidence of liquid crystalline phase formation. Optical microscopy showed that while the nanoparticle aggregates primarily partitioned toward the bottom surface of the sample, the nanowires self-assemble into seemingly endless birefringent strands that weave through multiple focal planes. These strands become light and dark as the sample is rotated relative to the polarizer. Figure 2a shows a representative image of a single focal plane under partially crossed polarizers. Imaging of successive focal planes failed to reveal any ends; the strands appear to be continuous. As shown by Figure 2b, the Ag−EG biphasic morphology is strikingly similar to the so-called "spaghetti" liquid crystal domain morphology which has only previously been reported for biphasic dispersions of 500 nm long SWNTs in 102−120% H_2SO_4.[17] The fact that similar morphologies were seen in these two markedly different systems suggests that there is an underlying physics dictating the formation of these unusual strandlike liquid crystalline domains. A key difference between both SWNTs and Ag nanowires and the "rodlike" polymers which form well-characterized globular domains[1] is their remarkably large persistence lengths. The persistence length of rodlike polymers such as poly(γ-benzyl-L-glutamate) (PBLG) is on the order of nanometers.[1] In contrast, the diameter-dependent persistence length of SWNTs is known to range from ~30 to 170 μm based on both particle tracking measurements[44] and calculations of $L_p = \kappa/(k_bT)$, where $\kappa = CD^3/8$ for hollow rods and C = 345 N/m based on the in-plane stiffness of carbon nanotubes.[45] For solid rods, $\kappa = ED^4/64$ where E is the Young's modulus. The Young's modulus of Ag nanowires is fairly constant at a value of ~80 GPa for 60 nm < D < 100 nm.[46] Therefore, for $D \sim 100$ nm, the persistence length of the Ag nanowires can be estimated to be on the order of 10^7 μm in the absence of defects. While nanowire breakage during repeated centrifugation suggests the presence of defects, the persistence length and the persistence length to contour length ratio are likely to be significantly higher than those of rodlike polymers or even SWNTs.

Attractive interactions are also likely a contributing factor to strandlike morphology. For SWNTs in superacids, the strandlike morphology was observed in the biphasic region of SWNT−102% H_2SO_4 where there were attractive interactions between SWNTs.[5] In contrast, the biphasic morphology was found to become more globular in SWNT−$HClSO_3$ where the attraction between SWNTs was nearly entirely mediated by the acid's protonating power.[37] Estimation of the attractive van der Waals (vdW) potential W for Ag nanowires in EG, under the assumption of nonretarded interactions with pairwise additivity,[18] shows that they are also attractive. For two parallel cylinders of equal dimension, W is expressed as

$$W = -\frac{A_{121} L R^{1/2}}{24 X^{3/2}} \quad (2)$$

where R is the average rod radii, L the average length, X the inter-rod separation distance, and A_{121} the appropriate Hamaker constant. For identical Ag particles interacting across water, A_{121} was reported to be 149 zJ.[47] We also find this value of A_{121} to be reasonable for describing Ag interacting across EG in accordance with the Lifshitz theory (see Supporting Information). The value of X was taken considering the limit of a single monolayer of solvent between nanowires having an effective diameter of ~0.3 nm. However, this solvent spacing is negligible when considering the adsorbed PVP layer surrounding the rod circumference

(44) Duggal, R.; Pasquali, M. *Phys. Rev. Lett.* **2006**, *96*(24), 246104.

(45) Yakobson, B. I.; Couchman, L. S. Carbon Nanotubes: Supramolecular Mechanics. In *Dekker Encyclopedia of Nanoscience and Nanotechnology*; Schwarz, J. A., Contescu, C. I., Putyera, K., Eds.; Marcel Dekker: New York, 2004; pp 587−601.

(46) Guofeng, W.; Xiaodong, L. *J. Appl. Phys.* **2008**, *104*(11), 113517.

(47) Bell, N. S.; Dimos, D. B. Calculation of Hamaker constants in non-aqueous fluid media. Materials Research Society Spring 2000 Meeting, San Francisco, CA, 2000; p 6.

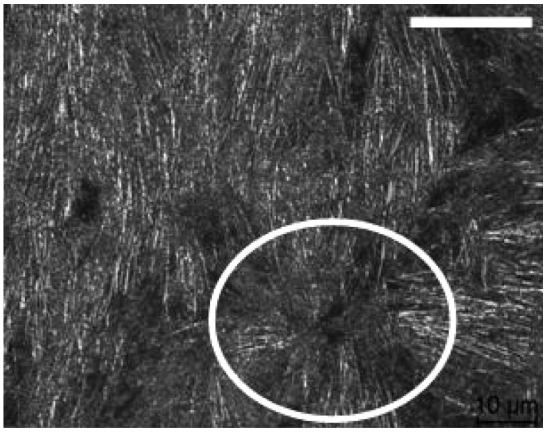

Figure 3. 0.42 vol % (4 wt %) silver in ethylene glycol (Ag−EG). At this concentration, a polydomain structure and no isotropic regions are observed. The circled region highlights the brushes of a disclination. The scale bar is 50 μm.

with thickness on the order of 10^1 nm (see Supporting Information). If one considers the PVP layer to behave as a barrier serving only to separate the rods (i.e., hard rod interactions between PVP layers on adjacent rods with long-range vdW attraction between Ag nanorods), the interaction energy between two parallel nanocylinders in close contact ($X = 10^1$ nm) is 7×10^{-18} J. In order to parametrize the magnitude of this interaction, we scaled the potential with respect to the magnitude of thermally induced Brownian forces (k_bT) and found W/k_bT to be on the order of 10^3 (10^1 for crossed cylinders), indicating the coated rods are interacting.[48] Future investigations of silver and other nanowire systems in multiple solvents should provide additional insights into the role of persistence length and attractive interactions on morphology of high aspect ratio rigid nanocylinders and perhaps lead to theories for predicting morphology.

Increasing the concentration of the sedimented Ag−EG through centrifugation and removal of the supernatant, but without the addition of other solvents, showed the expected reduction in the fraction of isotropic regions and an increase in the fraction of birefringent domains. At ~4 wt % silver, as measured by TGA, the sample was entirely birefringent; no isotropic regions could be observed even at the sample meniscus. At this concentration, a polydomain structure was observed where the domain size was much greater than the size of the individual rods (Figure 3). In addition, disclinations or Schlieren structures could be observed in the sample. These structures provide further evidence of liquid crystallinity[1,49] and have also been observed in other nanocylinder liquid crystals such as oxidized MWNTs in water,[49] goethite nanorods in water,[10] and SWNTs in 102% H_2SO_4.[17] The silver concentration of 4 wt % is the total concentration of both nanoparticle aggregates and nanowires and corresponds to 0.42 vol % based on the relative density of ethylene glycol and silver. For noninteracting monodisperse cylinders of $L = 6.8$ μm and $D = 100$ nm, Onsager theory predicts that ϕ_n is 4.49 vol %, over an order of magnitude higher than the concentration determined by optical microscopy. For most real, polydisperse, systems consisting solely of solvent dispersed rods, Onsager theory typically underpredicts ϕ_n. However, theoretical and experimental investigations of systems comprised of both rods and spheres show exceptionally complex phase behaviors which depend on both the concentrations and

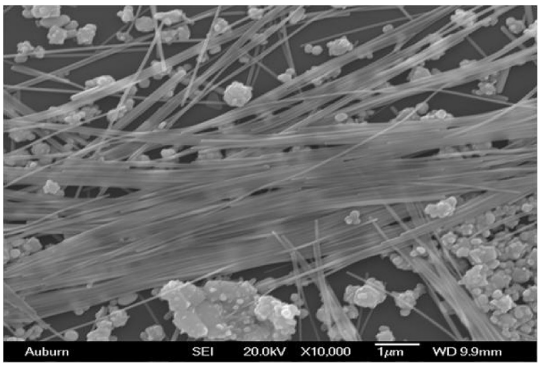

Figure 4. SEM image dried dispersion showing evidence of demixed nematic phase formation. The nanowires form aligned regions separate from the nanoparticle aggregates which tend to concentrate on the lower sample surface.

relative sizes of the rods and spheres.[50−54] Theoretical studies of liquid crystalline systems containing both rods and spheres[51,52] show that due to depletion effects the concentration induced disorder−order transition can result in either a mixed nematic state where the spheres are integrated into nematic domains formed by the cylinders or a demixed nematic state where separate rod-rich and sphere-rich phases form. The large diameter of the spherical nanoparticle aggregates relative to the nanowire diameter should result in a demixed nematic,[50] and imaging of the dispersions and quenched samples is consistent with demixed nematic phase formation. In biphasic samples such as those shown in Figure 2, the aggregates tend to concentrate closer to the bottom of the sample. No aggregates were visible in Figure 3, presumably they were hidden below the nanowire-rich aligned domains. SEM of a dried biphasic sample shows a similar result; the nanowire-rich aligned regions are separate and generally above the nanoparticle aggregate-rich regions (Figure 4). In demixed nematics, the spherical particles surrounding the rod-rich liquid crystalline domains serve to stabilize nematic phase formation and significantly reduce the concentration required for liquid crystalline phase formation. Therefore, the low transition concentration is in general agreement with the formation of a demixed nematic.

Although there is a wealth of literature on characterizing lyotropic dispersions of rodlike polymers through multiple characterization techniques,[1,55,56] optical microscopy is often used as a sole indicator of liquid crystallinity in dispersions of nanocylinders.[57] However, optical microscopy results are generally only qualitative and do not provide a quantitative indication of the phase boundaries or definitive proof that the rods are surrounded by solvent and capable of flow. Additional characterization of systems consisting of inorganic nanowires and spheres is complicated by the wide range of length scales, optical opacity at high concentrations, and the time and expense involved in producing large sample quantities. SEM, TEM, or AFM imaging of dried dispersions is often used as further supporting evidence,[13,14,58] but it is often difficult to deconvolute the effects of

(48) Solomon, M.; Spicer, P. *Soft Matter* **2010**, *6*(7), 1391–1400.
(49) Song, W. H.; Windle, A. H. *Macromolecules* **2005**, *38*(14), 6181–6188.
(50) Urakami, N.; Imai, M. *J. Chem. Phys.* **2003**, *119*(4), 2463–2470.
(51) Dogic, Z.; Frenkel, D.; Fraden, S. *Phys. Rev. E* **2000**, *62*(3), 3925–3933.
(52) Cuetos, A.; Martinez-Haya, B.; Lago, S.; Rull, L. F. *Phys. Rev. E* **2007**, *75*(6).
(53) Adams, M.; Dogic, Z.; Keller, S. L.; Fraden, S. *Nature* **1998**, *393*(6683), 349–352.
(54) Adams, M.; Fraden, S. *Biophys. J.* **1998**, *74*(1), 669–677.
(55) Marrucci, G. Rheology of Nematic Polymers. In *Liquid Crystallinity in Polymers*; Ciferri, A., Ed.; VCH Publishers: New York, 1991; pp 395−421.
(56) Kiss, G.; Porter, R. S. *J. Polym. Sci., Part B: Polym. Phys.* **1980**, *18*(2), 361–388.
(57) Li, L. S.; Marjanska, M.; Park, G. H. J.; Pines, A.; Alivisatos, A. P. *J. Chem. Phys.* **2004**, *120*(3), 1149–1152.
(58) Meuer, S.; Fischer, K.; Mey, I.; Janshoff, A.; Schmidt, M.; Zentel, R. *Macromolecules* **2008**, *41*(21), 7946–7952.

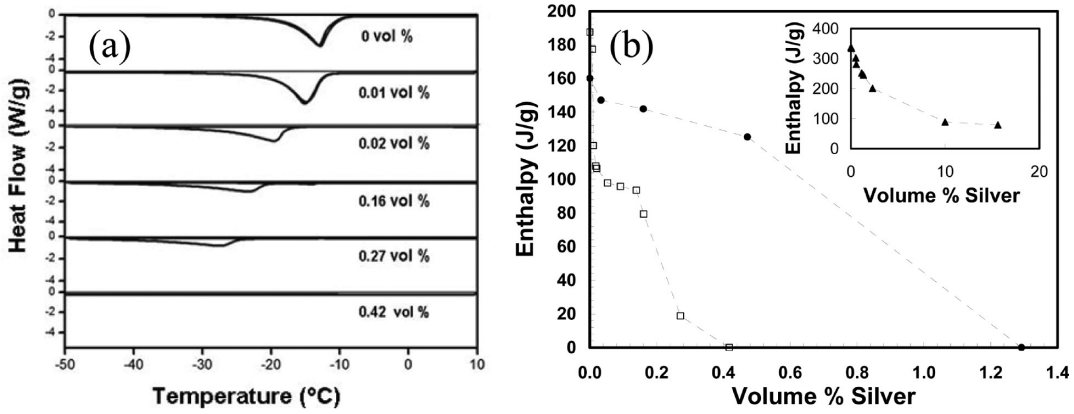

Figure 5. Differential scanning calorimetry of silver dispersions. (a) The shift in melting temperature and decrease in enthalpy for successively higher concentrations of Ag−EG obtained through centrifugation and sampling the centrifuge tube sidewall. (b) Plot of enthalpy vs volume fraction for Ag−EG from the centrifuge tube sidewall shown in (a) (squares), a different region of the sidewall (circles), and the entire sediment of samples transferred to water Ag−H_2O (inset). Dashed lines are merely intended to guide the eye.

surface interactions, capillary forces, and flow and concentration gradients resulting from contact line pinning (coffee stain formation).[59] X-ray scattering has been used to evaluate phase behavior in lyotropic goethite[10] and rutile[60] nanorod dispersions, but X-ray studies can be time-consuming, the equipment is not always readily available, and results can be affected by the nanocylinder length, polydispersity, and presence of other shapes. In the case of SWNTs, differential scanning calorimetry (DSC)[61] and rheology[17] were found to correlate with microscopy and X-ray data. To the authors' knowledge, however, these methods have not been explored for characterizing the phase behavior of dispersions containing high aspect ratio inorganic nanowires in the presence of nanoparticles.

DSC has the advantages of requiring very little sample and fairly rapid characterization time. Detection of liquid crystalline phase formation using DSC hinges on the interactions between the mesogen and solvent being such that ordering of the mesogens drives an accompanying ordering of the solvent.[61] DSC analysis of increasing concentrations of silver in three dispersions were explored. As shown in Figure 5a, pure ethylene glycol shows a melting peak centered at −15 °C with an enthalpy of 188 J/g. As the concentration of silver is increased, the melting point shifts to a lower temperature and the enthalpy decreases. For rod-enriched dispersions, the enthalpy initially decreases dramatically to a value of 106 J/g at a concentration of only 0.02 vol % Ag. The enthalpy then remains fairly constant at concentrations up to 0.14 vol %. This plateau behavior may be related to percolation of the nanowires or demixing of the sample into a nanowire-rich and nanoparticle-rich aggregate-rich phase. Above 0.14 vol % the enthalpy decreases rapidly again; at a concentration of 0.42 vol % no melting peak is observed, suggesting that all the solvent is ordered. This provides further support for optical microscopy observation that ϕ_n = 0.42 vol % Ag based on the absence of isotropic regions and the presence of Schlieren structures. As shown in Figure 5b, slightly changing the sampling location results in the same trend but different quantitative values. This highlights that the phase behavior is influenced by the relative amounts of rods and spheres and not simply

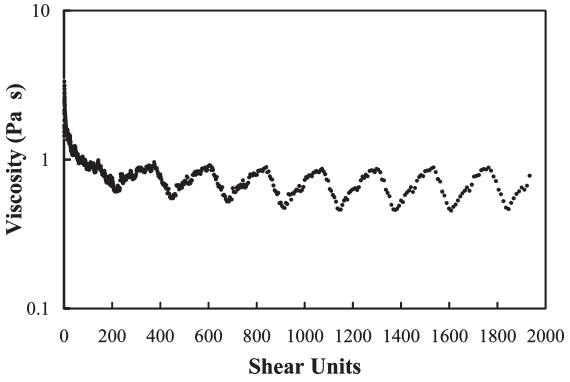

Figure 6. Start-up of flow for biphasic Ag−H_2O dispersion showing long oscillatory transients at a constant shear rate of 1 s^{-1}.

interactions with the solvent. On the other hand, retaining the entire sediment of the samples transferred to water results in an initial, but significantly more gradual, decrease in enthalpy with concentration followed by a plateau (inset Figure 5b). These results are in agreement with the qualitative optical microscopy results that long-range ordering in water required much higher concentrations than in ethylene glycol; all samples tested contained isotropic regions.

Rheological studies have been well established for determining the phase behavior of rodlike polymers[34,55] and have also proven useful for lyotropic SWNT−superacid dispersions.[17] Rheology has the advantages of probing the microstructure of a bulk sample of a dispersion and not being affected by optical opacity. However, rheological characterization has two key disadvantages in terms of the characterization of inorganic nanowire dispersions. First, even in the dilute regime, rotational relaxation time[3] scales with L^3; therefore, the time to obtain steady state measurements on the 6 μm long nanowire is over a 1000 times longer than the time required for a 500 nm long single-walled carbon nanotube. Second, while the scalability of inorganic nanowire syntheses is steadily improving, the amount of material required for rheological characterization is fairly large, particularly if one wishes to characterize oscillatory and steady shear behavior for a range of concentrations spanning the dilute, semidilute, biphasic, and liquid crystalline regimes. Nonetheless, rheology is useful for evaluating whether the sample meets the criteria that a liquid crystal must be able to flow and evaluating the sample stability over time. In this work biphasic samples of Ag−EG and Ag−H_2O

(59) Nobile, C.; Carbone, L.; Fiore, A.; Cingolani, R.; Manna, L.; Krahne, R. *J. Phys.: Condens. Matter* **2009**, *21* (26).
(60) Dessombz, A.; Chiche, D.; Davidson, P.; Panine, P.; Chaneac, C.; Jolivet, J. P. *J. Am. Chem. Soc.* **2007**, *129*(18), 5904–5909.
(61) Zhou, W.; Heiney, P. A.; Fan, H.; Smalley, R. E.; Fischer, J. E. *J. Am. Chem. Soc.* **2005**, *127*(6), 1640–1641.

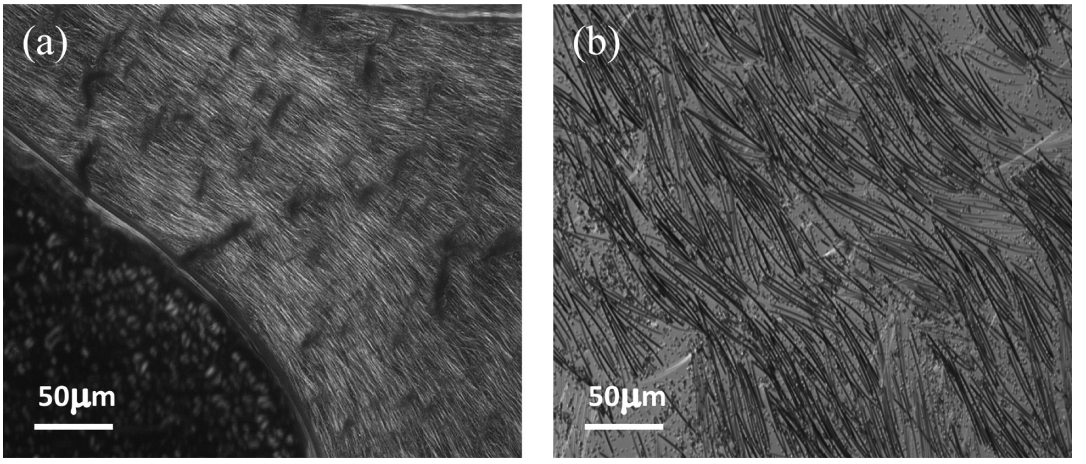

Figure 7. Optical microscopy images of shear alignment of (a) biphasic Ag−EG and (b) isotropic Ag−H_2O.

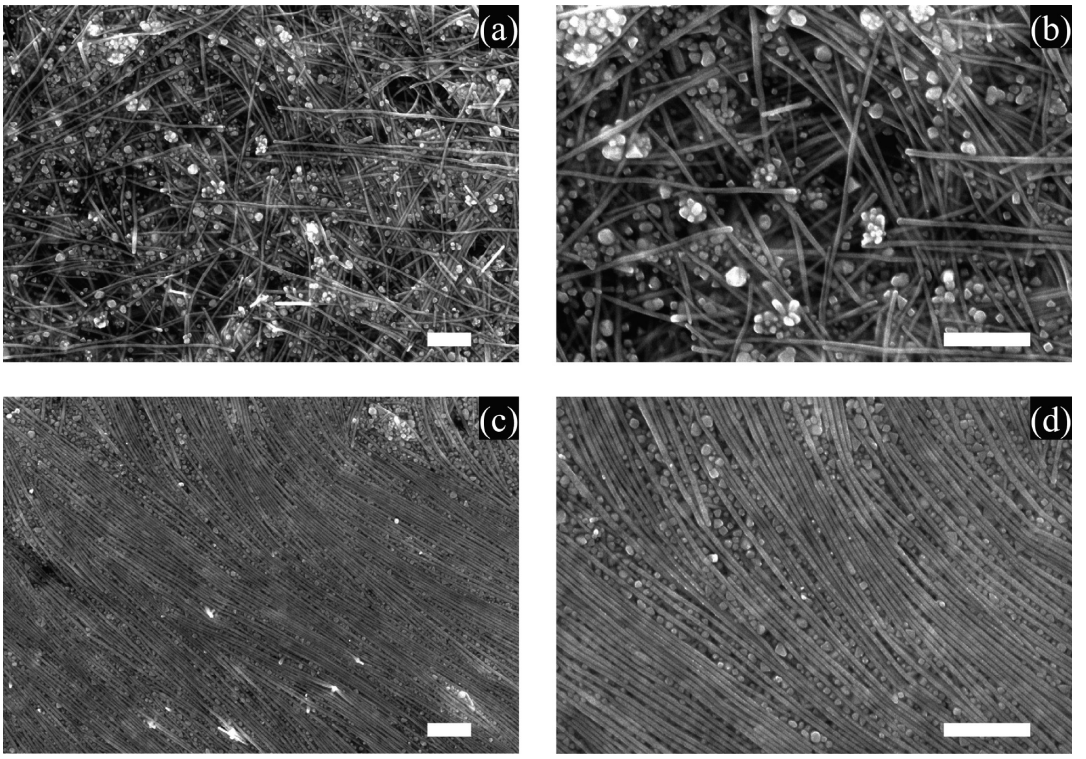

Figure 8. Scanning electron microscopy images of sheared and dried samples from Ag−H_2O dispersions showing a lower degree of alignment and demixing at lower concentrations: (a, b) initial concentration 0.16 vol % (1.7 wt %); (c, d) initial concentration 0.88 vol % (8.5 wt %). Magnifications are 10 000× in (a, c) and 20 000× in (b, d). All scale bars are 1 μm.

were characterized for their response to the start-up of shear. For an isotropic fluid, the start-up of shear typically results in an overshoot in the viscosity, followed by steady state in less than 100 shear units where a shear unit is defined as the product of shear rate and time. For both Ag−EG and Ag−H_2O dispersions, the response was an overshoot followed by very uniform oscillatory transients which persisted for over 1000 shear units.[55] For example, Figure 6 shows the response of Ag−H_2O 0.47 vol % (4.8 wt %) after start-up of shear at 1 s^{-1}. These results show that the sample is stable enough against sedimentation for rheological characterization. The presence of an overshoot after the start-up of shear followed by long oscillatory transients is one of the features associated with lyotropic rodlike polymer dispersions and has also been observed for SWNT−102% H_2SO_4 dispersions.[17] The regular oscillations are suggestive of a tumbling nematic.[34]

Shear Response and Processing into Coatings. Processing of liquid crystalline dispersions to form coatings, films, or fibers typically involves the application of shear; therefore, it is important to understand the shear response of the systems. While shear alignment of rods in fluid is well-known,[34] shearing liquid crystalline dispersions typically results in greater alignment than shearing isotropic dispersions.[1,36,62] Manually shearing biphasic Ag−EG dispersions with a coverslip at shear rates on the order of 500 s^{-1} based on the ∼30 μm gap and using a stopwatch to time the rate of coverslip motion results in a significant amount of ordering while shearing isotropic dispersions of Ag−H_2O results in much less uniform ordering (Figure 7). Shear

(62) Zamora-Ledezma, C.; Blanc, C.; Maugey, M.; Zakri, C.; Poulin, P.; Anglaret, E. *Nano Lett.* **2008**, *8*(12), 4103–4107.

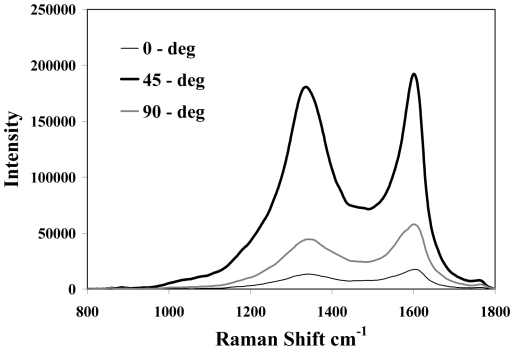

Figure 9. Polarization dependence of Raman spectra at various angles with respect to the electric field vector.

of biphasic dispersions also increases segregation of the nanoparticle aggregates and nanowires. Sharma et al. also observed increased nanoparticle nanorod separation resulting from the capillary flow associated with drop-drying gold dispersions on TEM grids.[15]

Similarly, removing the solvent after shear results in aligned silver coatings. Figure 8 shows SEM images at 10 000× and 20 000× of Ag−H_2O dispersions dried after applying the same shear. As observed for other systems, the higher degree of alignment in the coating was achieved when there was more initial alignment in the dispersion.[62] As shown in Figure 8a,b, applying shear to predominantly isotropic Ag−H_2O dispersions (ϕ = 0.16 vol %) results in little alignment. However, as shown in Figure 8c, d, the same method results in significant alignment when starting from largely birefringent Ag−H_2O dispersions with ϕ = 0.88 vol %. Furthermore, higher concentrations show a greater extent of nanowire−spherical aggregate demixing; at the higher concentration, the system is almost fully demixed after shear with the aligned nanowires ordering themselves above the spherical aggregates.

While SEM provides a visual picture of the degree of alignment, each image can only provide information about a limited area. Polarized Raman spectroscopy is routinely used for establishing the relative orientation of carbon nanotube films and fibers.[36,63,64] In this method, the relative degree of alignment is determined by taking the ratio of signature peak intensities with the sample aligned parallel and perpendicular to the laser. The PVP monolayer coating of the silver nanowires enables similar analysis. As shown in Figure 9, the intensity of the PVP peaks change as a rotating stage is used to change the orientation of the sample relative to the laser. In this case, the highest orientation is at 45°. Based on the relative intensities of the PVP peaks at ∼1600 cm^{-1}, the I^0/I^{45} ratio is 11:1 for the samples shown in Figure 8c,d, indicating a significant degree of alignment; this compares to less than 2:1 for the samples shown in Figure 8a,b.

(63) Saito, R.; Takeya, T.; Kimura, T.; Dresselhaus, G.; Dresselhaus, M. S. *Phys. Rev. B* **1998**, *57*(7), 4145.
(64) Haggenmueller, R.; Gommans, H. H.; Rinzler, A. G.; Fischer, J. E.; Winey, K. I. *Chem. Phys. Lett.* **2000**, *330*(3−4 SU), 219–225.

Conclusions

This work provides a foundation for coupled liquid crystalline self-assembly and flow alignment of high aspect inorganic nanowire dispersions. We have demonstrated liquid crystalline phase formation in a highly polydisperse system of silver nanowires and spherical nanoparticle agglomerates dispersed in ethylene glycol or water. In accordance with theory, the system form a demixed nematic where a spherical nanoparticle aggregate-rich phase stabilizes formation of nematic nanowire domains at an order of magnitude lower concentration than predicted by Onsager theory. Shearing predominantly isotropic dispersions results in little demixing or alignment. However, shearing predominantly liquid crystalline dispersions results in coatings with significant alignment and demixing. Such aligned coatings have potential applications as SERS substrates and antimicrobial coatings.

Acknowledgment. This research was supported by a National Science Foundation Nanoscale Exploratory Research Grant (CMMI-0707981) and CAREER Grant (CMMI-0846629). The authors thank Lauren Lamere and Jennifer Boice for assistance with synthesis experiments at different microwave conditions. We also thank Dr. Micah Green and Dr. Curtis Shannon for useful discussions.

Supporting Information Available: Images of the effect of microwave heating time on dispersion color, relative size of the nanoparticle aggregates, and separation after centrifugation; table showing nanoparticle aggregate and nanowire dimensions after various processing techniques; and discussion of Hamaker constant approximation. This material is available free of charge via the Internet at http://pubs.acs.org.